De Haas–van Alphen effect under rotation

Shu-Yun Yang,[1] Ren-Da Dong,[1] De-Fu Hou,[1,*] and Hai-Cang Ren[2,1,†]

[1]*Institute of Particle Physics and Key Laboratory of Quark and Lepton Physics (MOS), Central China Normal University, Wuhan 430079, China*

[2]*Physics Department, The Rockefeller University, 1230 York Avenue, New York, New York 10021-6399, USA*

(Received 7 February 2023; accepted 30 March 2023; published 24 April 2023)

We explored the interplay between magnetic field and rotation in the de Hass–van Alphen oscillation. The effect is found to be reduced because of the reweighting of different angular momentum states within the same Landau level by rotation energy. The implications of our results on high energy physics and condensed matter physics are discussed.

DOI: 10.1103/PhysRevD.107.076020

I. INTRODUCTION

The experimental activities for recent years regarding the polarization [1–7] and chiral magnetic effects [8–10] in off-central relativistic heavy ion collisions promoted theoretical research interests in a rotating thermodynamic system in a magnetic field [11–18]. The same physical conditions are also present in a neutron star [19–22]. One of the interplays between magnetism and rotation, the Barnett effect (or Einstein–de Haas effect) [23–25] has been considered in hydrodynamic modeling of the collisions. In this work, we examine another interplay between magnetism and rotation, i.e. the de Haas–van Alphen effect [26,27] in a strongly degenerate rotating Fermi gas. Though purely theoretical at the present stage, the implications are expected to shed light on the magnetic properties of the quark matter core, if it exists, in a neutron star and/or the Quark Gluon Plasma (QGP) droplet generated in the RHIC STAR fixed target experiment, where the quark density and temperature are toward the strong degeneracy. The conclusion may also be tested directly in condensed matter physics.

The de Haas–van Alphen (dHvA) effect in a strongly degenerated system of charged fermions is the consequence of filling discrete but highly degenerate Landau levels in a magnetic field. The degeneracy of each Landau level is proportional to the transverse area of the system with respect to the direction of the constant magnetic field, and the degeneracy per unit area is proportional to the magnitude of the magnetic field. The spacing between successive Landau levels also increases with the magnetic field. When the system is static, all degenerate states within a Landau level are equally probable to be occupied. Varying the strength of the magnetic field will cause a large number of fermions (proportional to the transverse area) to jump between different discrete Landau levels, resulting in oscillatory dependence of the thermodynamic functions and transport coefficients on the magnetic field. Among them are the magnetization and magnetic susceptibility that correspond to the first order and second order derivatives of the thermodynamic pressure calculated in this work with respect to the magnetic field. Since its discovery in 1930 [28,29], the de Haas–van Alphen effect has been serving a powerful tool to detect the Fermi sea of electrons in metals. The theoretical derivation of the de Haas–van Alphen effect in a nonrotating system in terms of the Landau gauge can be found in many textbooks, e.g. [30,31] for nonrelativistic fermions and in [32] for relativistic fermions.

When the system is in rotation, the thermodynamic equilibrium is established under a nonzero macroscopic angular momentum. The equal distribution of different angular momentum states within a Landau level is offset by the nonzero angular velocity with higher angular momenta more favored than lower ones, which amounts to lifting the degeneracy of the Landau level. The dHvA oscillation is thereby expected to be reduced by rotation. Consider a cylindrical volume of radius R in a constant magnetic field parallel to its symmetry axis, designated as the z-axis, the states of each fermion are characterized by the z-component of the momentum q, the z-component of the angular momentum M, and the radial quantum number

*Corresponding author.
houdf@mail.ccnu.edu.cn

†Corresponding author.
haicang117@gmail.com

of the wave function $n(\geq 0)$. A Landau level corresponds to $M > 0$, the cyclotron motion in classical picture, and is characterized by n. All $M > 0$ within the same Landau level are degenerate up to $M \sim eBR^2$ when the center of the cyclotron orbit reaches the boundary. When the cylinder is rotating about the z-axis at a constant angular velocity $\omega(> 0)$, the angular momentum states within the same Landau level but with different M are no longer equally favored because of the Boltzmann factor $e^{M\omega/T}$ in the ensemble of a macroscopic angular momentum. On the other hand, the requirement of subluminal linear speed on the boundary limits the radius of the cylinder $R < 1/\omega$, and the ideal thermodynamic limit $R \to \infty$ cannot be reached. The degeneracy of the Landau levels is always finite, proportional to the transverse area of the cylinder. We shall take the thermodynamic approximation by retaining the leading term in power in $1/R$ in the thermodynamic pressure, keeping in mind $\omega R = O(1)$,[1] and a sharp cutoff in the summation over angular momentum states within a Landau level is introduced to take care of the finite size effect of the spectrum. Consequently, the implication of the rotation in the dHvA oscillation depends on the size of the system and the angular velocity. As we shall see, the dHvA is completely suppressed for typical parameters appropriate in a neutron star but may lead to an observable effect for a cold and dense QGP fireball created in a future RHIC project. For a strongly degenerate nonrelativistic electron gas, the reduction of the dHvA is detectable in a rotating metallic sample.

This paper is organized as follows. In Sec. II, the dHvA term of the thermodynamic pressure of a rotating ultrarelativistic quark gas is calculated and its implications are discussed. The same effect for a nonrelativistic electron is examined in Sec. III. Section IV concludes the paper.

II. ULTRARELATIVISTIC FERMI GAS

A. Solution of Dirac equation in cylindrical coordinate

For a massless fermion of electric charge e in a constant magnetic field $\vec{B} = B\hat{z}$, the Hamiltonian in chiral representation reads

$$H = -i\vec{\alpha}\cdot(\vec{\nabla} - ieA) = \begin{pmatrix} -i\vec{\sigma}\cdot(\vec{\nabla} - ieA) & 0 \\ 0 & i\vec{\sigma}\cdot(\vec{\nabla} - ieA) \end{pmatrix}, \quad (1)$$

where the vector potential

$$\vec{A} = \frac{1}{2}\vec{B}\times\vec{r}. \quad (2)$$

We adopt the circular gauge instead of the Landau gauge for the convenience of investigating a Fermi gas rotating about the z-axis. As the fermions of opposite chiralities have identical spectra, we shall focus on one of them with the Hamiltonian in what follows:

$$H = -i\vec{\sigma}\cdot(\vec{\nabla} - ieA), \quad (3)$$

and the eigenvalue equation $H\chi = E\chi$. For the ansatz of the two-component wave function χ in cylindrical coordinates, i.e.

$$\chi(\vec{r}) = \begin{pmatrix} f(\rho)e^{i(M-\frac{1}{2})\phi} \\ g(\rho)e^{i(M+\frac{1}{2})\phi} \end{pmatrix} e^{iqz}, \quad (4)$$

we have the equations for the radial functions $f(\rho)$ and $g(\rho)$

$$\begin{cases} qf(\rho) - i\left(\frac{d}{d\rho} + \frac{M+\frac{1}{2}}{\rho} - \frac{1}{2}eB\rho\right)g(\rho) = Ef(\rho) \\ -i\left(\frac{d}{d\rho} - \frac{M-\frac{1}{2}}{\rho} + \frac{1}{2}eB\rho\right)f(\rho) - qg(\rho) = Eg(\rho) \end{cases}, \quad (5)$$

where q and M are the eigenvalue of the momentum and total angular momentum in the direction of the magnetic field with $M = \pm 1/2, \pm 3/2, \ldots$. Equation (5) can be solved in terms of the generalized Laguerre polynomial $L_n^{\mu}(z)$, and we end up with the normalized wave function [33]

$$\chi_{nMqs}(\vec{r}) = \frac{1}{2\pi}\sqrt{\frac{n!}{(n+m)!}}e^{-\frac{\zeta}{2}} \begin{pmatrix} \sqrt{\frac{eB(E+q)}{2E}}\zeta^{\frac{m}{2}}L_n^m(\zeta)e^{im\phi} \\ \frac{iseB}{\sqrt{E(E-q)}}\zeta^{m+1}L_{n-1}^{m+1}(\zeta)e^{i(m+1)\phi} \end{pmatrix} e^{iqz} \quad (6)$$

for $M > 0$, and

[1] In this case the kinetic energy of rotation grows with the volume, such as other extensive thermodynamic quantities.

$$\chi_{nMqs}(\vec{r}) = \frac{1}{2\pi}\sqrt{\frac{n!}{(n+|m|)!}}e^{-\frac{\zeta}{2}}\begin{pmatrix} \sqrt{\frac{eB(E+q)}{2E}}\zeta^{\frac{|m|}{2}}L_n^{|m|}(\zeta)e^{im\phi} \\ -\frac{iseB(n+|m|)}{\sqrt{E(E-q)}}\zeta^{\frac{(|m|-1)}{2}}L_n^{|m|-1}(\zeta)e^{i(m+1)\phi}\end{pmatrix}e^{iqz} \tag{7}$$

for $M<0$, where $\zeta \equiv \frac{1}{2}eB\rho^2$, $m \equiv M-1/2$, $n=0,1,2,\ldots$, and $s=\pm$. The corresponding eigenvalue of energy is $E=sE_{nMq}$ with

$$E_{nMq} = \begin{cases} \sqrt{2neB+q^2} & \text{for } M>0 \\ \sqrt{2(n+|m|)eB+q^2} & \text{for } M<0 \end{cases}. \tag{8}$$

Care must be exercised for the case $n=0$ of the solution (6) because of the nonexistence of L_{-1}^{m+1} and the singularity at $E=-q$. For $E=\pm q$, Eq. (5) becomes

$$\begin{cases} \left(\frac{d}{d\rho}+\frac{m+1}{\rho}-\frac{1}{2}eB\rho\right)g(\rho) = i(\pm q-q)f(\rho) \\ \left(\frac{d}{d\rho}-\frac{m}{\rho}+\frac{1}{2}eB\rho\right)f(\rho) = i(\pm q+q)g(\rho). \end{cases} \tag{9}$$

A normalizable solution exists only if $E=q$ and reads

$$\chi_{0Mqs}(\vec{r}) = \frac{2^{m+1}}{\sqrt{\pi}}(eB)^{\frac{m+1}{2}}\rho^m e^{-\frac{1}{4}eB\rho^2+im\phi+iqz}\begin{pmatrix}1\\0\end{pmatrix} \tag{10}$$

with $s=\mathrm{sign}(q)$, which implies the up (down) mover for a positive (negative) energy solution. The wave function (7) corresponds to the classical motion along the cyclotron orbit and the upper $M>0$ spectrum on the right-hand side (RHS) of (8) constitutes the entire set of Landau levels and is responsible for bulk magnetic properties including de Haas–van Alphen effect to be discussed below in thermodynamic approximation. The wave function (7) and the spectrum (8) are specific to the cylindrical coordinates and are subleading in the thermodynamic approximation as we shall see below.

B. Thermodynamic pressure

The Hamiltonian of a massless fermion field in a magnetic field is given by

$$\mathcal{H} = \int d^3\vec{r}\psi^\dagger H\psi, \tag{11}$$

where H is the single particle Hamiltonian (3) and the field operator

$$\psi(\vec{r}) = \sum_{nMq}\eta_{nM}(q)(a_{nMq}\chi_{nMq+}(\vec{r}) + b_{nM-q}^\dagger\chi_{nMq-}(\vec{r})), \tag{12}$$

where

$$\eta_{nM}(q) = \begin{cases}\theta(q) & \text{for } M>0 \text{ and } n=0 \\ 1 & \text{otherwise}\end{cases}. \tag{13}$$

We have

$$\mathcal{H} = \sum_{n,M,q}\eta_{nM}(q)E_{nMq}(a_{nMq}^\dagger a_{nMq} + b_{nMq}^\dagger b_{nMq}). \tag{14}$$

Correspondingly, the fermion number operator

$$\begin{aligned} Q &= \int d^3\vec{r}\psi^\dagger\psi \\ &= \sum_{n,M,q}\eta_{nM}(q)(a_{nMq}^\dagger a_{nMq} - b_{nMq}^\dagger b_{nMq}), \end{aligned} \tag{15}$$

and the angular momentum projection operator

$$\begin{aligned} J_z &= \int d^3\vec{r}\psi^\dagger\left(-i\frac{\partial}{\partial\phi}+\frac{1}{2}\sigma_z\right)\psi \\ &= \sum_{n,M,q}\eta_{nM}(q)M(a_{nMq}^\dagger a_{nMq} - b_{nMq}^\dagger b_{nMq}). \end{aligned} \tag{16}$$

Consequently, the thermodynamic pressure at temperature T and chemical potential μ of a system rotating about the z-axis with an angular velocity $\omega(>0)$ is

$$\begin{aligned} P = {} & \frac{T}{\Omega}\sum_{n=0,M>0,q>0}[\ln(1+e^{-\beta(|q|-M\omega-\mu)})+\ln(1+e^{-\beta(|q|+M\omega+\mu)})] + \frac{T}{\Omega}\sum_{n\neq0,M>0,q}\left[\ln\left(1+e^{-\beta(\sqrt{q^2+2neB}-M\omega-\mu)}\right)\right. \\ & \left.+\ln\left(1+e^{-\beta(\sqrt{q^2+2neB}+M\omega+\mu)}\right)\right] + \frac{T}{\Omega}\sum_{n\neq0,M>0,q}\left[\ln\left(1+e^{-\beta(\sqrt{q^2+2(n+M+\frac{1}{2})eB}+M\omega-\mu)}\right)\right. \\ & \left.+\ln\left(1+e^{-\beta(\sqrt{q^2+2(n+M+\frac{1}{2})eB}-M\omega+\mu)}\right)\right], \end{aligned} \tag{17}$$

where we have switched the sign of M of the lower branch of the spectrum (8) for clarity. For a cylinder of radius R and length L, the spatial volume $\Omega = \pi R^2 L$,

$$\sum_{n,M,q}(\cdots) = \frac{1}{\pi R^2}\int_{-\infty}^{\infty}\frac{dq}{2\pi}\sum_{n,M}(\cdots). \tag{18}$$

As stated in the Introduction, the ideal thermodynamic limit is prohibited because of the requirement $v \equiv \omega R < 1$. Instead we shall take the thermodynamic approximation for sufficiently large R by sorting the terms according to its power, keeping in mind that $\omega R = O(1)$. For a finite R summation over M is limited. It follows from Eqs. (6) and (7) that the square of the wave function for large M and finite n is peaked at the maximum of $\rho^{2|m|}\exp(-\frac{1}{2}eB\rho^2)$, which gives rise to $\rho^2 = 2|m|/(eB)$. When this ρ becomes comparable with R, the finite size effect will distort the spectrum (8). Therefore, we introduce a cutoff for the summation over M, i.e.

$$M \le M_c = \left[\frac{1}{2}eBR^2\right] \gg 1, \tag{19}$$

with $[\cdots]$ truncating its argument inside its integer part. As will be shown below, this cutoff reproduces the dHvA effect derived from the Landau gauge in the absence of rotation. Without solving the boundary value problem near the boundary, we assume the uncertainty $\delta M_c = O(1)$ of the cutoff.

Assuming strong degeneracy, $\mu \gg T$, the antiparticle contributions may be ignored[2] and we end up with

$$\begin{aligned}P =& \frac{T}{\pi R^2}\int_0^{\infty}\frac{dq}{4\pi}\sum_{M>0}\ln(1+e^{-\beta(|q|-M\omega-\mu)})\\ &+\frac{T}{\pi R^2}\int_{-\infty}^{\infty}\frac{dq}{2\pi}\sum_{n>0,M>0}\ln(1+e^{-\beta(\sqrt{q^2+2neB}-M\omega-\mu)})\\ &+\frac{T}{\pi R^2}\int_{-\infty}^{\infty}\frac{dq}{2\pi}\sum_{n,M>0}\ln(1+e^{-\beta(\sqrt{q^2+2(n+M+\frac{1}{2})eB}+M\omega-\mu)}),\end{aligned} \tag{20}$$

where the contribution of the lowest Landau level has been isolated from higher Landau levels because of different integration domains of q. The summation over M in the third term of (20) converges in the limit $M_c \to \infty$ and thereby does not contribute to the thermodynamic limit, and we are left with the Landau level terms only, i.e.

$$\begin{aligned}P =& \frac{T}{\pi R^2}\int_0^{\infty}\frac{dq}{4\pi}\sum_{M>0}\ln(1+e^{-\beta(|q|-M\omega-\mu)})\\ &+\frac{T}{\pi R^2}\int_{-\infty}^{\infty}\frac{dq}{2\pi}\sum_{n>0,M>0}\ln(1+e^{-\beta(\sqrt{q^2+2neB}-M\omega-\mu)})\\ \equiv& \frac{1}{\pi R^2}\sum_{M>0}P_M,,\end{aligned} \tag{21}$$

where

$$\begin{aligned}P_M =& T\int_0^{\infty}\frac{dq}{4\pi}\ln(1+e^{-\beta(|q|-\mu_M)})\\ &+T\int_{-\infty}^{\infty}\frac{dq}{2\pi}\sum_{n>0}\ln(1+e^{-\beta(\sqrt{q^2+2neB}-\mu_M)}),\end{aligned} \tag{22}$$

with $\mu_M = \mu + M\omega$.

C. de Haas–van Alphen oscillation

As the standard derivation of the de Haas–van Alphen (dHvA) effect, the summation over the Landau level index n can be carried out with the aid of the Poisson formula

$$\sum_{n=0}^{\infty}f(n) = \int_0^{\infty}f(n)dn + 2\mathrm{Re}\sum_{l=1}^{\infty}\int_0^{\infty}f(n)e^{2i\pi ln}dn. \tag{23}$$

We have

$$P_M = F_{0M} + 2\mathrm{Re}\sum_{l=1}^{\infty}F_{lM}, \tag{24}$$

where

$$F_{lM} = T\int_{-\infty}^{\infty}\frac{dq}{2\pi}\int_0^{\infty}dne^{i2\pi ln}\ln(1+e^{-\beta(\sqrt{q^2+2neB}-\mu_M)}). \tag{25}$$

The dHvA oscillation resides in the second term of (24), and we shall focus on it.

Transforming the integration variables from q, n to q, ϵ with $\epsilon = \sqrt{q^2+2neB}$, we find, via twice integration by part with respect to ϵ, that

$$F_{lM} = \mathrm{I}_{lM} + \mathrm{II}_{lM} + \mathrm{III}_{lM} \tag{26}$$

for $l > 0$, where

$$\mathrm{I}_{lM} = i\frac{eBT}{4\pi^2 l}\int_{-\infty}^{\infty}dq\ln(1+e^{-\beta(q-\mu_M)}), \tag{27}$$

[2]To be cautious, let us examine whether the combination $\mathcal{E} \equiv \sqrt{q^2+2(n+M+\frac{1}{2})eB} - M\omega$ in the last term of (17) can become negative and compete with μ for large M. For the maximum $M(=M_c)$, $\mathcal{E} > \sqrt{2M_c eB} - M_c\omega \simeq e\mathrm{BR}(1-v/2) > 0$. The approximation of dropping the antiparticle contribution appears safe.

$$\mathrm{II}_{lM} = \frac{eB}{4i\pi^2 l}\sqrt{\frac{eB}{\pi l}}\int_{-\infty}^{\infty} dq e^{-i\frac{l\pi}{eB}q^2}\frac{\phi\left(\sqrt{\frac{l\pi}{eB}}|q|\right)}{e^{\beta(q-\mu_M)}+1}, \tag{28}$$

and

$$\mathrm{III}_{lM} = -\frac{eB}{4i\pi^2 l}\sqrt{\frac{eB}{l\pi}}\int_0^{\infty} d\epsilon\phi\left(\sqrt{\frac{l\pi}{eB}}\epsilon\right) \times \frac{\beta e^{\beta(\epsilon-\mu_M)}}{[e^{\beta(\epsilon-\mu_M)}+1]^2}\int_{-\epsilon}^{\epsilon} dq e^{-i\frac{l\pi}{eB}q^2}, \tag{29}$$

with

$$\phi(z) \equiv \int_z^{\infty} dx e^{ix^2}. \tag{30}$$

I_{lM} is imaginary and thereby does not contribute to (24). Assuming the condition

$$T \ll \sqrt{eB} \ll \mu, \tag{31}$$

the leading terms of II_{lM} and III_{lM} can be worked out, and we obtain that

$$\mathrm{II}_{lM} = \frac{eB}{4\pi^3 l^2}\left[\ln\left(\sqrt{\frac{4l\pi}{eB}}\mu_M\right)+\frac{1}{2}\gamma_E - i\frac{\pi}{4}\right], \tag{32}$$

with $\gamma_E = 0.5772\ldots$ the Euler constant (see Appendix A for the derivation), and

$$\mathrm{III}_{lM} = -\frac{(eB)^{\frac{1}{2}}T}{4\pi}\frac{e^{i\left(\frac{l\pi^2}{eB}\mu_M^2-\frac{\pi}{4}\right)}}{l^{3/2}\sinh\frac{2l\pi^2 T(\mu+M\omega)}{eB}}, \tag{33}$$

where the integration formula

$$\int_{-\infty}^{\infty} dx \frac{e^{x+i\alpha}}{(e^x+1)^2} = \frac{\pi\alpha}{\sinh\pi\alpha} \tag{34}$$

and the asymptotic form

$$\phi(z) = \frac{i}{2z}e^{iz^2} + \cdots \text{for } z \to \infty \tag{35}$$

have been employed to reduce III_M. The dHvA oscillation stems from III_M. Summing over M, we end up with the dHvA term of the thermodynamic pressure under rotation, i.e.

$$P_{\mathrm{dHvA}} \equiv \frac{1}{\pi R^2}\sum_{M>0}\left(2\mathrm{Re}\sum_{l=1}^{\infty}\mathrm{III}_{lM}\right) = -\frac{(eB)^{\frac{1}{2}}}{2\pi^2 R^2}\sum_{l=1}^{\infty}\frac{1}{l^{3/2}}\sum_{M>0}\frac{\cos\left[\frac{l\pi}{eB}(\mu+M\omega)^2-\frac{\pi}{4}\right]}{\sinh\frac{2l\pi^2 T(\mu+M\omega)}{eB}}. \tag{36}$$

In the absence of rotation, $\omega = 0$, Eq. (36) becomes

$$P_{\mathrm{dHvA}} = -\frac{T(eB)^{\frac{3}{2}}}{4\pi^2}\sum_{l=1}^{\infty}\frac{1}{l^{3/2}}\frac{\cos\left[\frac{l\pi}{eB}\mu^2-\frac{\pi}{4}\right]}{\sinh\frac{2l\pi^2 T\mu}{eB}} \overset{T\to 0}{\to} \frac{(eB)^{\frac{5}{2}}}{8\pi^4\mu}\sum_{l=1}^{\infty}\frac{1}{l^{5/2}}\cos\left[\frac{l\pi}{eB}\mu^2-\frac{\pi}{4}\right], \tag{37}$$

in agreement with the expression derived from the Landau gauge.

Equation (36) can be further simplified at zero temperature, i.e.

$$P_{\mathrm{dHvA}} = -\frac{(eB)^{\frac{3}{2}}}{4\pi^4 R^2}\sum_{M>0}\frac{1}{\mu+M\omega} \times \sum_{l=1}^{\infty}\frac{1}{l^{5/2}}\cos\left[\frac{l\pi}{eB}(\mu+M\omega)^2-\frac{\pi}{4}\right]. \tag{38}$$

Assuming $\omega \ll \sqrt{eB}$, the rapid convergence of the infinite series with respect to l enables us to approximate the summation over M by an integral. Consequently

$$\begin{aligned} P_{\mathrm{dHvA}} &\simeq -\frac{(eB)^{\frac{3}{2}}}{4\pi^4 R^2\omega}\int_{\mu}^{\mu+M_c\omega} dx\frac{1}{x}\sum_{l=1}^{\infty}\frac{1}{l^{5/2}}\cos\left(\frac{l\pi}{eB}x^2-\frac{\pi}{4}\right) \\ &= -\frac{(eB)^{\frac{3}{2}}}{8\sqrt{2}\pi^4 R^2\omega}\sum_{l=1}^{\infty}\frac{1}{l^{5/2}}\left[\mathrm{Ci}\left(\frac{l\pi}{eB}(\mu+M_c\omega)^2\right)-\mathrm{Ci}\left(\frac{l\pi}{eB}\mu^2\right)+\mathrm{Si}\left(\frac{l\pi}{eB}(\mu+M_c\omega)^2\right)-\mathrm{Si}\left(\frac{l\pi}{eB}\mu^2\right)\right] \\ &\simeq \frac{(eB)^{\frac{5}{2}}}{8\pi^5 R^2\omega}\sum_{l=1}^{\infty}\frac{1}{l^{7/2}}\left[\frac{\sin\left(\frac{l\pi}{eB}\mu^2-\frac{\pi}{4}\right)}{\mu^2}-\frac{\sin\left(\frac{l\pi}{eB}(\mu+M_c\omega)^2-\frac{\pi}{4}\right)}{(\mu+M_c\omega)^2}\right], \end{aligned} \tag{39}$$

where $\mathrm{Ci}(z)$ and $\mathrm{Si}(z)$ are cosine and sine integrals and their asymptotic forms for $z \gg 1$, i.e.

$$\begin{cases} \mathrm{Si}(z) \approx \frac{\pi}{2} - \frac{\cos z}{z} \\ \mathrm{Ci}(z) \approx \frac{\sin z}{z} \end{cases}, \tag{40}$$

are employed in the last step. If the maximum rotation energy $M_c\omega$ dominates, i.e. $M_c\omega \gg \mu$, the second term of (39) can be dropped. we have

$$P_{\mathrm{dHvA}} \simeq \frac{(eB)^{\frac{5}{2}}}{8\pi^5\mu^2R^2\omega}\sum_{l=1}^{\infty}\frac{1}{l^{7/2}}\sin\left(\frac{l\pi}{eB}\mu^2 - \frac{\pi}{4}\right), \tag{41}$$

and the uncertainty of M_c does not contribute.

D. Numerical estimates

As pointed out in the Introduction, the rotation will lift the degeneracy of states within each Landau level and thereby reduce the de Haas–an Alphen oscillation. In this section, we shall estimate the amount of reduction using the parameters appropriate for two realistic rotating ultrarelativistic fermion systems in a magnetic field, the quark matter core, and a QGP droplet at high baryon density. Since the Fermi gas approximation of these two systems tends to be poor and the condition of the latter system is highly transient, we are not attempting to model the two systems. The significance of our result below is only in the sense of the order of magnitude. For the ultrarelativistic system, we shall use $m_\pi = 140$ MeV as the scale of the chemical potential and temperature and $m_\pi^2 = 10^{18}$ G as the scale of the magnetic field. The dimensionless ratio P_{dHvA}/P_0 under different conditions will be plotted in the rest of this subsection, where $P_0 = \mu^4/(24\pi^2)$ is the thermodynamic pressure in the absence of a magnetic field and rotation.

1. The quark matter core of a neutron star

The radius of a neutron star is of the order of 10 km, and we assume a quark matter core made of light flavors of smaller radius R with a chemical potential of several hundreds of MeV, i.e. a few times of pion's rest energy, m_π. The magnetic field inside a neutron star can reach as high as 10^{15} G, i.e. $1.4 \times 10^{-3}m_\pi^2$. Even for the fastest spinning neutron star, PSR J1748-2446ad, when the angular velocity is 716 Hz, the linear speed at the boundary of the core is $v \simeq 0.015 \ll 1$ (in the unit of the speed of light). Consequently

$$\frac{\mu}{M_c\omega} = \frac{\mu}{m_\pi}\cdot\frac{m_\pi^2}{eB}\cdot\frac{10^{-16}}{\mathrm{R(km)v}} \ll 1, \tag{42}$$

$$\frac{\omega}{\sqrt{eB}} \simeq 2.2 \times 10^{-20}\frac{m_\pi}{\sqrt{eB}} \ll 1 \tag{43}$$

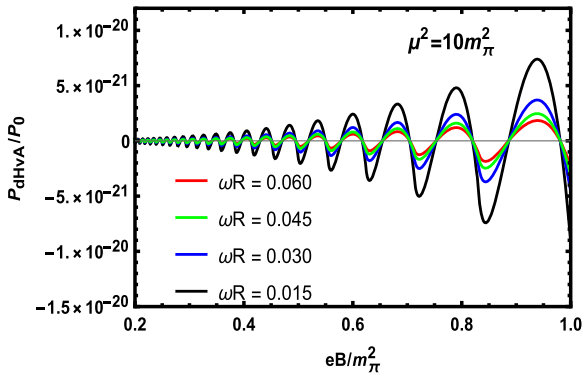

FIG. 1. The dHvA oscillation with respect to the magnetic field when $T = 0$. Here, $m_\pi = 140$ MeV, the chemical potential $\mu^2 = 10m_\pi^2$, and the radius is $R = 1$ km.

for a typical neutron star. The approximation underlying (41) is thereby justified, and we estimate

$$\frac{P_{\mathrm{dHvA}}}{P_{\mathrm{dHvA}}\|_{\omega=0}} \sim \frac{2}{\mu Rv} \simeq \frac{3.86 \times 10^{-16}}{\mu(\mathrm{MeV})R(\mathrm{km})v}, \tag{44}$$

leading to a huge suppression of dHvA oscillation.

The thermodynamic pressure at $\mu^2 = 10m_\pi^2$ and zero temperature versus magnetic field $0 < eB < 0.01m_\pi^2$ is plotted in Fig. 1 for several linear speeds at the boundary of the rotating cylinder of ultrarelativistic Fermi gas whose radius is comparable to a typical neutron star. As a benchmark, the thermodynamic pressure in the absence of rotation is displayed in Fig. 2. The effect is suppressed by 17 orders of magnitude.

2. A cold and dense QGP droplet

The suppression of dHvA in a neutron star may be attributed to its large size. Let us switch to the parameter values appropriate to a cold and dense QGP droplet where the suppression of dHvA oscillation with the angular velocity becomes modest. The dHvA term of the thermodynamic pressure of Eq. (39) for $R = 10$ fm versus the

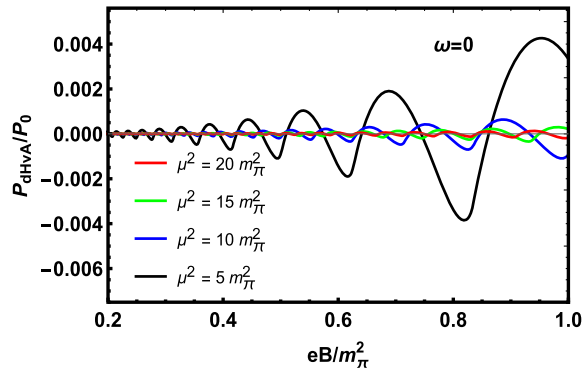

FIG. 2. The dHvA oscillation with respect to the magnetic field. Here, $\omega = 0$ and $T = 0$.

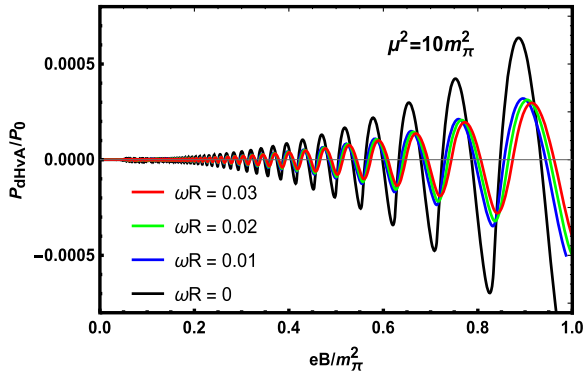

FIG. 3. The dHvA oscillation with respect to the magnetic field. Here, $T = 0$, we fix the chemical potential $\mu^2 = 10m_\pi^2$, and the radius is $R = 10$ fm.

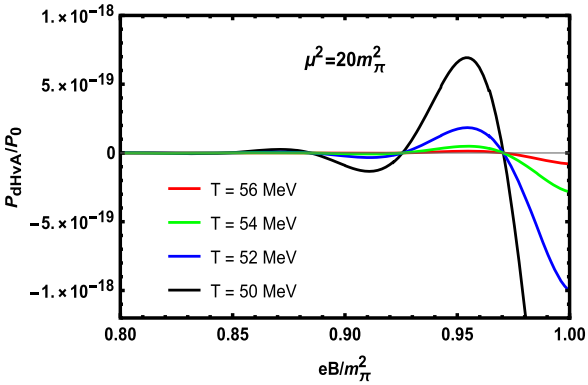

FIG. 4. The dHvA oscillation with respect to the magnetic field. Here, we fix the chemical potential $\mu^2 = 20m_\pi^2$, $\omega R = 0.01$, and the radius is $R = 10$ fm.

magnetic field at fixed chemical potential and temperature is plotted for several angular velocities including $\omega = 0$ in Fig. 3. The same equation at fixed chemical potential and a nonzero angular velocity is plotted for several temperatures in Fig. 4. The dHvA without rotation, Eq. (37), at the same chemical potential and the same set of temperatures is plotted in Fig. 5 for reference. Notice that the suppression

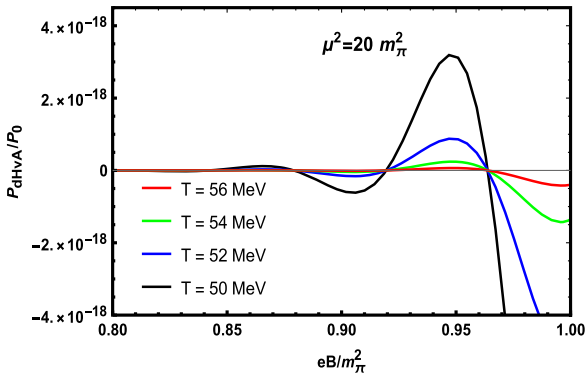

FIG. 5. The dHvA oscillation with respect to the magnetic field. Here, we fix the chemical potential $\mu^2 = 20m_\pi^2$, and $\omega = 0$.

of dHvA with temperature becomes milder with $\omega \neq 0$. The selection of the size and the magnetic field is motivated by the conditions of the current heavy ion collisions in RHIC and LHC.

While the RHIC STAR fixed target experiment is expected to generate QGP of lower energy and higher baryon density, i.e., closer to the density axis of the QCD phase diagram, there may still be a gap to meet the condition of the cold and dense QGP described above. Even if it did, the rapid expansion would hinder the observability of the effect because of nonequilibrium. So our discussions here are highly speculative.

III. NONRELATIVISTIC FERMI GAS

The Hamiltonian of a nonrelativistic electron in a constant magnetic field reads

$$H = -\frac{1}{2m_e}(\vec{\nabla} - ie\vec{A})^2 + \frac{1}{2}\sigma_z\omega_B, \tag{45}$$

with the vector potential

$$\vec{A} = \frac{1}{2}B\hat{z} \times \vec{r}, \tag{46}$$

where $\omega_B = eB/m_e$ is the cyclotron frequency and $\sigma_z = \text{diag.}(1, -1)$. The spectrum in cylindrical coordinates can be found in many textbooks of quantum mechanics and is given by

$$E_{nmq\sigma} = \frac{q^2}{2m_e} + \left(n + \frac{m - |m|}{2} + \frac{1}{2}\right)\omega_B + \frac{1}{2}\sigma\omega_B, \tag{47}$$

where q is the momentum along the z-direction, $n = 0, 1, 2, \ldots,$ are radial quantum numbers and $m = 0, \pm1, \pm2, \ldots, \pm M_c$ are the z-component of the orbital angular momentum and $\sigma = \pm$ labels spin projections. The corresponding wave function reads

$$\psi_{nmq\sigma}(\vec{r}) = \sqrt{\frac{n!eB}{2\pi(n + |m|)!L}}\zeta^{\frac{|m|}{2}}e^{-\frac{\zeta}{2}}L_n^{|m|}(\zeta)e^{i(m\phi+qz)}. \tag{48}$$

In a cylinder of finite radius, the thermodynamic approximation limits the azimuthal quantum number as (19), i.e.

$$|m| < m_c = \left[\frac{1}{2}eBR^2\right] \gg 1, \tag{49}$$

with an uncertainty $\delta m_c = O(1)$ as in the ultrarelativistic case. The Landau levels correspond to $m \geq 0$ and are labeled by n.

A. Thermodynamic pressure and dHvA

For a free nonrelativistic electron gas, the dHvA can be extracted using the same Poisson formula (23) as in most of the textbooks of solid-state physics. Here we adopt a more elegant approach via Mellin transformation [31].

The thermodynamic pressure of the electron gas in a rotating cylindrical volume of radius R and length L reads

$$P = \frac{1}{\pi R^2}\sum_m P_m(\zeta_m), \tag{50}$$

where

$$P_m(\zeta_m) = \frac{T}{L}\sum_{n,q,\sigma}\ln\left(1+\frac{1}{\zeta_m}e^{-\beta E_{qnm\sigma}}\right), \tag{51}$$

with $\omega > 0$ the angular velocity and

$$\zeta_m = e^{-\beta(\mu+m\omega)}. \tag{52}$$

The case of strong degeneracy corresponds to $\zeta_m \ll 1$. The Mellin transformation of the function $P_m(\zeta)$ with respect to ζ is given by

$$\begin{aligned} Q(s) &= \int_0^\infty d\zeta \zeta^{s-1} P_m(\zeta) \\ &= \frac{\pi T}{Ls\sin\pi s}\sum_{n,q,\sigma} e^{-s\beta(E_{nmq\sigma}-\frac{1}{2}\sigma\omega)} \end{aligned} \tag{53}$$

for $0 < \mathrm{Re}s < 1$. The last equality follows from integration by part and the formula

$$\int_0^\infty dx \frac{x^{s-1}}{x+1} = \frac{\pi}{\sin\pi s}. \tag{54}$$

For the same reason as in the relativistic case, the contribution from $m < 0$ is subleading in the thermodynamic approximation, and we focus only on the branch $m \geq 0$ of the spectrum. We have for $m \geq 0$

$$\begin{aligned} Q(s) &= \frac{\pi T}{Ls\sin\pi s}\sum_q e^{-\frac{s\beta q^2}{2m_e}}\sum_{n,\sigma} e^{-(n+\frac{1}{2})s\beta\omega_B-\frac{1}{2}\sigma s\beta(\omega_B-\omega)} \\ &= \frac{\pi T}{\lambda s^{3/2}\sin\pi s}\frac{\cosh\frac{1}{2}s\beta(\omega_B-\omega)}{\sinh\frac{1}{2}s\beta\omega_B}, \end{aligned} \tag{55}$$

where $\lambda = \sqrt{2\pi/(mT)}$ is the thermal wavelength. It follows from the Mellin inversion formula that

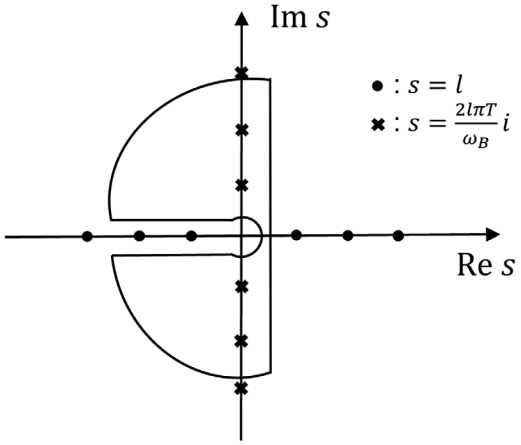

FIG. 6. Contour integration [31].

$$P_m(\zeta) = \int_{c-i\infty}^{c+i\infty}\frac{ds}{2\pi i}\zeta^{-s}Q(s) \tag{56}$$

with $0 < c < 1$. The integrand on the complex s-plane consists of a branch cut running along the negative real axis, poles along both real and imaginary axes, i.e.

$$s = l, \qquad s = \frac{2l\pi T}{\omega_B} i, \tag{57}$$

with $l = 0, \pm 1, \pm 2, \ldots$. Closing the contour from the left as shown in Fig. 6 for $\zeta < 1$, we find

$$P_m(\zeta) = \mathrm{I}_m(\zeta) + \mathrm{II}_m(\zeta), \tag{58}$$

where I_m is the integral around the branch cut and II_m stems from the poles along the imaginary axis. The former contributes to the Landau diamagnetism and Pauli paramagnetism along with the Barnett effect, and the latter gives rise to dHvA oscillation. Summing up the residues of the poles within the contour, we end up with

$$\begin{aligned} \mathrm{II}_m(\zeta_m) = \frac{2T}{\lambda}\sqrt{\frac{\omega_B}{2\pi T}}\sum_{l=1}^\infty \frac{1}{l^{3/2}}\mathrm{csch}\frac{2l\pi^2 T}{\omega_B}\cos\frac{l\pi\omega}{\omega_B} \\ \times\cos\left[\frac{2l\pi(\mu+m\omega)}{\omega_B}-\frac{\pi}{4}\right]. \end{aligned} \tag{59}$$

Summing up the orbital angular momentum, we obtain that

$$P_{\mathrm{dHvA}} = \frac{1}{\pi R^2}\sum_{m=0}^{m_c}\mathrm{II}_m = -\frac{T(m_e\omega_B)^{1/2}}{\pi^2 R^2}\sum_{l=1}^\infty \cos\frac{l\pi\omega}{\omega_B}\frac{\sin\left(\frac{2l\pi\mu}{\omega_B}-\frac{l\pi\omega}{\omega_B}-\frac{\pi}{4}\right)-\sin\left(\frac{2l\pi\mu}{\omega_B}+\frac{l\pi\omega}{\omega_B}-\frac{\pi}{4}+\frac{2l\pi m_c\omega}{\omega_B}\right)}{l^{3/2}\sinh\frac{2l\pi^2 T}{\omega_B}\sin\frac{l\pi\omega}{\omega_B}}. \tag{60}$$

Without rotation, $\omega = 0$, the well-known dHvA formula

$$P_{\mathrm{dHvA}}|_{\omega=0} = -\frac{T(m_e\omega_B)^{3/2}}{2\pi^2}\sum_{l=1}^{\infty}\frac{1}{l^{3/2}}\mathrm{csch}\frac{2l\pi^2 T}{\omega_B}\cos\left(\frac{2l\pi\mu}{\omega_B}-\frac{\pi}{4}\right) \tag{61}$$

recovers. At zero temperature, Eq. (60) becomes

$$\begin{aligned} P_{\mathrm{dHvA}}|_{T=0} &= -\frac{(m_e\omega_B)^{3/2}}{4\pi^4 m_e R^2}\sum_{l=1}^{\infty}\cos\frac{l\pi\omega}{\omega_B}\frac{\sin\left(\frac{2l\pi\mu}{\omega_B}+\frac{l\pi\omega}{\omega_B}-\frac{\pi}{4}+l\pi m_e\omega R^2\right)-\sin\left(\frac{2l\pi\mu}{\omega_B}-\frac{l\pi\omega}{\omega_B}-\frac{\pi}{4}\right)}{l^{5/2}\sin\frac{l\pi\omega}{\omega_B}} \\ &\simeq -\frac{(m_e\omega_B)^{5/2}}{4\pi^5 m_e^2\omega R^2}\sum_{l=1}^{\infty}\frac{1}{l^{7/2}}\left[\sin\left(\frac{2l\pi\mu}{\omega_B}-\frac{\pi}{4}+\frac{2l\pi m_c\omega}{\omega_B}\right)-\sin\left(\frac{2l\pi\mu}{\omega_B}-\frac{\pi}{4}\right)\right], \end{aligned} \tag{62}$$

where the approximation $\omega \ll \omega_B$ is made for the typical parameters in condensed matter physics. This expression is to be compared with the zero temperature limit of (63), i.e.

$$P_{\mathrm{dHvA}}|_{\omega=0} = -\frac{(m_e\omega_B)^{5/2}}{4\pi^4 m_e}\sum_{l=1}^{\infty}\frac{1}{l^{5/2}}\cos\left(\frac{2l\pi\mu}{\omega_B}-\frac{\pi}{4}\right). \tag{63}$$

At this point, it is interesting to compare the nonrelativistic dHvA and the ultrarelativistic dHvA. As shown in Eq. (47), given q and σ, the nonrelativistic Landau levels ($m > 0$) are equally spaced while the spacing between successive ultrarelativistic Landau levels in the upper spectrum on the RHS of Eq. (8) decreases with increasing n. Since the dHvA is sensitive to the energy levels around the chemical potential μ, the amplitude of the oscillation is expected to be independent of μ in the nonrelativistic case but decreases with μ in the ultrarelativistic case as reflected in the large μ suppression by $\sinh\frac{2l\pi^2 T\mu}{eB}$ of (37) in the latter case. When rotation is turned on, the effective chemical potential increases with the angular momentum quantum number. Consequently, the nonrelativistic dHvA appears less vulnerable than the ultrarelativistic one.

B. Numerical estimates

The electron gas in a good metal at room temperature, $T \sim (1/40)$ eV, can be well approximated by a free Fermi in the strong degeneracy limit. The chemical potential is 1–10 eV, which makes $\mu/T \sim 40 \sim 400 \gg 1$ and the zero temperature approximation works well. For a magnetic field up to a few Teslas and an angular velocity in Hertz, we have

$$\omega/\omega_B \simeq 5.57\times 10^{-12}\frac{\omega(\mathrm{Hz})}{\mathrm{B(T)}}, \tag{64}$$

justifying the approximation made in (62) for mechanical rotation achievable in the laboratory. The same condition also makes the contribution of the uncertainty in the angular momentum cutoff m_c to the phase of the oscillation in (60) and (62) negligible.

The dHvA oscillation is expected to be significantly reduced when the largest rotation energy $m_c\omega$ within a Landau level exceeds the spacing between successive levels, ω_B. With R in centimeters, the linear velocity of the circumference $v = \omega R$ in terms of cm/s, it follows from (49) that

$$\frac{m_c\omega}{\omega_B} \simeq 0.43 R v, \tag{65}$$

independent of the magnetic field.

Parallel to the ultrarelativistic case, the dimensionless ratio P_{dHvA}/P_0 of a strongly degenerate electron gas versus magnetic field for a long cylinder of radius $R = 1$ cm at $T = 0$ is plotted in Figs. 7–9, where $P_0 = (2m_e\mu)^{5/2}/(15\pi^2 m_e)$ is the nonrelativistic pressure at $B = 0$ and $\omega = 0$. The magnetic field varies in a small neighborhood of 1T and the angular velocity is taken such that the RHS of (65) is of order one. The dHvA effect without rotation, Eq. (63), for different chemical potentials is shown in Fig. 7 as a benchmark. The parallel setup for $\omega R = 2$ cm/s, Eq. (62), is shown in Fig. 8 with similar profiles. More important is Fig. 9 where dHvA at different ωR is displayed. The suppression of the oscillation by rotation is evident and should be observable by measuring the magnetization and/or magnetic suspectibility

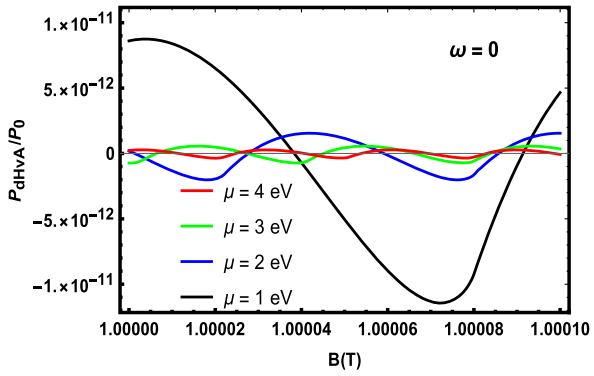

FIG. 7. The nonrelativistic dHvA oscillation with respect to the magnetic field when $T = 0$ and $\omega = 0$.

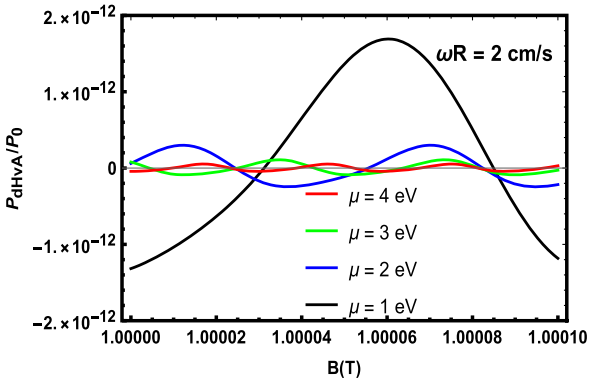

FIG. 8. The nonrelativistic dHvA oscillation with respect to the magnetic field when $T = 0$. Here, we fix $\omega R = 2$ cm/s and $R = 1$ cm.

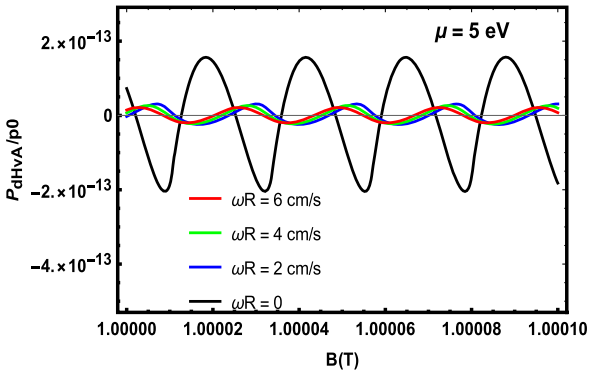

FIG. 9. The nonrelativistic dHvA oscillation with respect to the magnetic field when $T = 0$. Here, we fix the chemical potential $\mu = 5$ eV and the radius is $R = 1$ cm.

(derivatives of the thermodynamics pressure with respect to magnetic field) of a rotating metallic cylinder.

IV. CONCLUDING REMARKS

Let us recapitulate what we presented in the preceding sections. We examined the robustness of the de Haas–van Alphen effect in a strongly degenerate Fermi gas under rotation. We derived the analytical formulas for dHvA oscillation for a long cylinder rotating about its axis under a constant magnetic field parallel to the axis in the ultrarelativistic limit and nonrelativistic limit. As the macroscopic degeneracy (proportional to the transverse area) of Landau levels is offset by the rotation energy of states of different angular momentum within each Landau level. The amplitude of the oscillation is reduced. The amount of reduction depends on the angular velocity ω and the radius of the cylinder R, and the oscillation is expected to become insignificant for sufficiently large ω and R. The ultrarelativistic dHvA appears more vulnerable than the nonrelativistic one because of decreasing Landau level spacing with energy.

Applying the ultrarelativistic formula to estimate dHvA with typical parameters of a neutron star, and with typical parameters of a cold and dense QGP droplet, we noted that the dHvA oscillation is completely suppressed in the former case and remains in the latter. The nonrelativistic formula, on the other hand, showed that for a typical electron gas in a good metal, the variation of dHvA oscillation with angular velocity appears detectable, via magnetization and/or magnetic susceptibility.

As self-criticism, our approximation of the finite size effect by introducing the maximum angular momentum within a Landau level in (19) and (49) may be crude. Possible contribution from edge states [17] has not been considered. Limited by the analytical tractability, the cylindrical shape of the system is not suitable to model a neutron star or a QGP droplet. Though the effect is expected to remain for a Fermi liquid, the interaction in quark matter may modify significantly the quantitative prediction. In this sense, our result is very preliminary.

ACKNOWLEDGMENTS

We thank Ren-Hong Fang for the fruitful discussions. This work is supported in part by the National Key Research and Development Program of China under Contract No. 2022YFA1604900. This work is also partly supported by the National Natural Science Foundation of China (NSFC) under Grants No. 12275104, No. 11890711, No. 11890710, and No. 11735007.

APPENDIX

For $\mu \gg T$, Eq. (56) can be approximated as

$$\mathrm{II}_{lM} \simeq \frac{1}{2i\pi^2 l}\sqrt{\frac{eB}{l\pi}}\int_0^{\mu_M} dq e^{-i\frac{l\pi}{eB}q^2}\phi\left(\sqrt{\frac{l\pi}{eB}}q\right) = \frac{eB}{2i\pi^3 l^2}J, \tag{A1}$$

where

$$J = \int_0^K dx e^{-ix^2}\phi(x) = \int_0^K dx e^{-ix^2}\int_x^\infty d\xi e^{i\xi^2} \tag{A2}$$

with $K = \sqrt{\frac{l\pi}{eB}}\mu_M$. Introducing $\xi = xt$, we find

$$J = \int_0^K dx e^{-ix^2} x\int_1^\infty dt e^{it^2x^2} = \frac{1}{2i}\int_1^\infty dt\frac{e^{iK^2(t^2-1)}-1}{t^2-1}$$
$$= -\frac{1}{2}K^2\int_1^\infty dt e^{iK^2(t^2-1)} t\ln\frac{t-1}{t+1}, \tag{A3}$$

where the last equality follows from integration by part. Introducing $z = t^2 - 1$, we have

$$J = -\frac{1}{4}K^2 \int_0^\infty dz e^{iK^2 z} \ln \frac{\sqrt{z+1}-1}{\sqrt{z+1}+1}. \quad \text{(A4)}$$

If follows from the Jordan lemma that the integration path can be rotated to the imaginary axis on the z-plane, and we end up with

$$J = -\frac{i}{4}K^2 \int_0^\infty dy e^{-K^2 y} \ln \frac{\sqrt{1+iy}-1}{\sqrt{1+iy}+1}. \quad \text{(A5)}$$

For $K \gg 1$, we have

$$J \simeq -\frac{i}{4}K^2 \int_0^\infty dy e^{-K^2 y} \ln \frac{iy}{4} = \frac{i}{2}\left(\ln(2K) + \frac{1}{2}\gamma_E\right) + \frac{\pi}{8}. \quad \text{(A6)}$$

This gives rise to the RHS of (32).

[1] L. Adamczyk *et al.*, Global Λ hyperon polarization in nuclear collisions: evidence for the most vortical fluid, Nature (London) **548**, 62 (2017).

[2] B. I. Abelev *et al.*, Global polarization measurement in Au + Au collisions, Phys. Rev. C **76**, 024915 (2007); **95**, 039906(E) (2017).

[3] Jaroslav Adam *et al.*, Global polarization of Λ hyperons in Au + Au collisions at $\sqrt{s_{NN}} = 200$ GeV, Phys. Rev. C **98**, 014910 (2018).

[4] Jaroslav Adam *et al.*, Polarization of Λ ($\bar{\Lambda}$) Hyperons Along the Beam Direction in Au + Au Collisions at $\sqrt{s_{NN}} = 200$ GeV, Phys. Rev. Lett. **123**, 132301 (2019).

[5] Jaroslav Adam *et al.*, Measurement of inclusive J/ψ polarization in $p + p$ collisions at $\sqrt{s} = 200$ GeV by the STAR experiment, Phys. Rev. D **102**, 092009 (2020).

[6] J. Adam *et al.*, Global Polarization of Ξ and Ω Hyperons in Au + Au Collisions at $\sqrt{s_{NN}} = 200$ GeV, Phys. Rev. Lett. **126**, 162301 (2021).

[7] M. S. Abdallah *et al.*, Global Λ-hyperon polarization in Au + Au collisions at $\sqrt{s_{NN}} = 3$ GeV, Phys. Rev. C **104**, L061901 (2021).

[8] M. S. Abdallah *et al.*, Search for the Chiral Magnetic Effect via Charge-Dependent Azimuthal Correlations Relative to Spectator and Participant Planes in Au + Au Collisions at $\sqrt{s_{NN}} = 200$ GeV, Phys. Rev. Lett. **128**, 092301 (2022).

[9] M. S. Abdallah *et al.*, Pair invariant mass to isolate background in the search for the chiral magnetic effect in Au + Au collisions at $\sqrt{s_{NN}} = 200$ GeV, Phys. Rev. C **106**, 034908 (2022).

[10] Mohamed Abdallah *et al.*, Search for the chiral magnetic effect with isobar collisions at $\sqrt{s_{NN}} = 200$ GeV by the STAR Collaboration at the BNL Relativistic Heavy Ion Collider, Phys. Rev. C **105**, 014901 (2022).

[11] Francesco Becattini, Jinfeng Liao, and Michael Lisa, Strongly interacting matter under rotation: An introduction, Lect. Notes Phys. **987**, 1 (2021).

[12] Hao-Lei Chen, Kenji Fukushima, Xu-Guang Huang, and Kazuya Mameda, Analogy between rotation and density for Dirac fermions in a magnetic field, Phys. Rev. D **93**, 104052 (2016).

[13] Kenji Fukushima, Takuya Shimazaki, and Lingxiao Wang, Mode decomposed chiral magnetic effect and rotating fermions, Phys. Rev. D **102**, 014045 (2020).

[14] Koichi Hattori and Yi Yin, Charge Redistribution from Anomalous Magnetovorticity Coupling, Phys. Rev. Lett. **117**, 152002 (2016).

[15] Yizhuang Liu and Ismail Zahed, Rotating Dirac fermions in a magnetic field in 1 + 2 and 1 + 3 dimensions, Phys. Rev. D **98**, 014017 (2018).

[16] Emil Mottola and Andrey V. Sadofyev, Chiral waves on the Fermi-Dirac sea: Quantum superfluidity and the axial anomaly, Nucl. Phys. **B966**, 115385 (2021).

[17] M. N. Chernodub and Shinya Gongyo, Edge states and thermodynamics of rotating relativistic fermions under magnetic field, Phys. Rev. D **96**, 096014 (2017).

[18] M. N. Chernodub and Shinya Gongyo, Interacting fermions in rotation: Chiral symmetry restoration, moment of inertia and thermodynamics, J. High Energy Phys. 01 (2017) 136.

[19] R. Gonzalez Felipe, A. Perez Martinez, H. Perez Rojas, and M. Orsaria, Magnetized strange quark matter and magnetized strange quark stars, Phys. Rev. C **77**, 015807 (2008).

[20] Chinatsu Watanabe, Naotaka Yoshinaga, and Shuichiro Ebata, Equations of state for hadronic matter and mass-radius relations of neutron stars with strong magnetic fields, Universe **8**, 48 (2022).

[21] Pétri Jérôme, Particle acceleration and radiation reaction in a strongly magnetised rotating dipole, Astron. Astrophys. **666**, A5 (2022).

[22] Debarati Chatterjee, Jérôme Novak, and Micaela Oertel, Structure of ultra-magnetised neutron stars, Eur. Phys. J. A **57**, 249 (2021).

[23] A. Einstein and W. J. de Haas, Experimental proof of the existence of Ampère's molecular currents, in *Proceedings of Huygens Institute–Royal Netherlands Academy of Arts and Sciences (KNAW), 18 I, 1915, Amsterdam* (1915), pp. 696–711.

[24] Samuel J. Barnett, Gyromagnetic and electron-inertia effects, Rev. Mod. Phys. **7**, 129 (1935).

[25] Samapan Bhadury, Wojciech Florkowski, Amaresh Jaiswal, Avdhesh Kumar, and Radoslaw Ryblewski, Relativistic Spin Magnetohydrodynamics, Phys. Rev. Lett. **129**, 192301 (2022).

[26] Y. Ōnuki, Magnetic systems: De Haas–van Alphen studies of fermi surface, in *Encyclopedia of Materials: Science and*

Technology, edited by K. H. Jürgen Buschow, Robert W. Cahn, Merton C. Flemings, Bernhard Ilschner, Edward J. Kramer, Subhash Mahajan, and Patrick Veyssière (Elsevier, Oxford, 2001), pp. 4964–4968.

[27] W. Z. Jiang and N. Van Giai, Magnetic susceptibility oscillation in neutron stars with the hadron-quark transition, AIP Conf. Proc. **865**, 256 (2006).

[28] W. J. De Haas and P. M. Van Alphen, The dependence of the susceptibility of diamagnetic metals upon the field, in *Communication NO. 212a from the Physical Laboratory, Leiden* (1930).

[29] L. D. Landau, Diamagnetismus der metalle, Z. Phys. **64**, 629 (1930).

[30] L. D. Landau, E. M. Lifšic, E. M. Lifshitz, L. P. Pitaevskii, and M. J. Kearsley, Chapter 63—Statistical Physics: Theory of the Condensed State, *Course of Theoretical Physics* (Elsevier Science, New York, 1980).

[31] Huanwu Peng and Xiseng Xu, *Chapter 13.2—The Fundamentals of Theoretical Physics*, (Peking University Press, Beijing, 1998).

[32] Daniel Cangemi and Gerald V. Dunne, Temperature expansions for magnetic systems, Ann. Phys. (N.Y.) **249**, 582 (1996).

[33] Ren-Hong Fang, Thermodynamics for a rotating chiral fermion system in the uniform magnetic field, Symmetry **14**, 1106 (2022).